Journal of Alloys and Compounds 513 (2012) 18–22

Contents lists available at SciVerse ScienceDirect

Journal of Alloys and Compounds

journal homepage: www.elsevier.com/locate/jallcom

Letter

Surface plasmon enhanced blue–green photoluminescence from carbon-rich amorphous silicon carbide films

Zhe Li, Juncao Bian, Haiyan He, Zhaohui Ren, Xiwen Zhang*, Xiang Li, Gaorong Han**

State Key Laboratory of Silicon Materials, Department of Materials Science and Engineering, Zhejiang University, Hangzhou 310027, China

ARTICLE INFO

Article history:
Received 3 June 2011
Received in revised form 31 October 2011
Accepted 1 November 2011
Available online 9 November 2011

Keywords:
Thin films
Vapor deposition
Optical properties
Luminescence

ABSTRACT

Surface plasmons (SPs) have been utilized to enhance the luminescence efficiency of light-emitting materials and devices in the past decade. In this work, the enhanced photoluminescence (PL) from carbon-rich amorphous silicon carbide (a-$Si_{1-x}C_x$:H) films (with a PL peak at ~480 nm) has been achieved for the first time via coupling with SPs generated at the Ag/a-$Si_{1-x}C_x$:H interface. The enhancement factor was found to firstly increase with the Ag nanoparticle size, subsequently reach a maximum value of 3.3 when the average Ag nanoparticle size and the surface area coverage of Ag interlayers were 76 nm and 44% respectively, and eventually decrease as the Ag interlayers became continuous. It was found that such enhancement was mainly due to the SPs scattering. Since the carbon-based films have similar microstructure and PL mechanism to those of the carbon-rich a-$Si_{1-x}C_x$:H films, coupling with SPs has been proven to be a promising way to enhance the light emission from carbon-based films which can also be utilized for the large-area solid-state lighting applications.

1. Introduction

Since 1990, the idea of the surface plasmon (SP) enhanced light emission has been proposed and attracted a worldwide attention [1]. SPs are the collective oscillations of free electrons in a metal, which occur at the interfaces between metals and dielectrics [2]. In addition to the propagating surface plasmons (PSPs) on a plane surface, the collective oscillations of electrons in metal nanoparticles embedded in a dielectric matrix are localized surface plasmons (LSPs) [3,4]. Either PSP or LSP can interact with nearby light emitter through its evanescent or near-field coverage for enhancing emission [5]. In previous studies, Zn and Al were demonstrated to couple to deep UV photons due to high SP energy [6–8]. Au and Cu, which have similar optical and electronic properties, have found use in the red spectral region [7–9]. Ag was most commonly used in the visible spectral range as it has the lowest loss of SP energy in this region [10,11]. In recent years, PSPs and LSPs of Ag have been extensively studied to enhance the luminescence efficiency of light emitting materials and devices, such as InGaN/GaN [1,4,12,13], silicon quantum dots (Si-QD) [3,14], and ZnO films [15–19], for the applications of ultrabright light-emitting diodes (LEDs), or ultraviolet UV lasers. For example, Yeh et al. [13] have recently enhanced the InGaN/GaN LED emission intensity by 150% relative to a LED without an Ag layer. Kim et al. [3] reported a 4.3-fold EL enhancement of Si-QDs LED by QD-Ag coupling. In Cheng et al.'s [16] report on the ZnO films, a maximum photoluminescence (PL) enhancement factor of 3 was achieved via SPs. However, the materials aforementioned have been hardly used for the large-area solid-state lighting or processed on a flexible substrate. Therefore, amorphous silicon carbide films, which are potential ideal candidates for such purposes, have recently become the 'hot spot' in the relevant research community.

The hydrogenated amorphous silicon carbide (a-$Si_{1-x}C_x$:H) films, especially the ones with high carbon content which can emit visible PL at room temperature (RT), have been extensively studied in recent years due to its wide applications in micro-electronic, optoelectronic, and large-area electroluminescent devices [20–22]. Silicon carbide films have been prepared using different techniques, such as plasma enhanced chemical vapor deposition (PECVD) [21–24], hot wire CVD [25,26], laser CVD [27] or sputtering techniques [28,29], etc. Among these different processing methodologies, the use of reactive plasmas was found to be an effective way to obtain high deposition rates for a-$Si_{1-x}C_x$:H films [21]. The films prepared via PECVD from hydrogen diluted source gases have also been reported with superior photoelectric properties due to fewer defects, a much less clustered hydrogen phase and more ordered network [30]. Moreover, uniform films with sound electronic properties can be easily achieved over a large area by PECVD. Therefore, a-$Si_{1-x}C_x$:H has been considered to be an appropriate substance for the large-area solid-state lighting and flat-screen display devices. In addition, considering its compatibility with semiconductor integrated circuit

* Corresponding author. Tel.: +86 571 8827 6240; fax: +86 571 8827 6234.
** Corresponding author.
E-mail addresses: zhangxw@zju.edu.cn (X. Zhang), hgr@zju.edu.cn (G. Han).

0925-8388/$ – see front matter © 2011 Elsevier B.V. All rights reserved.
doi:10.1016/j.jallcom.2011.11.001

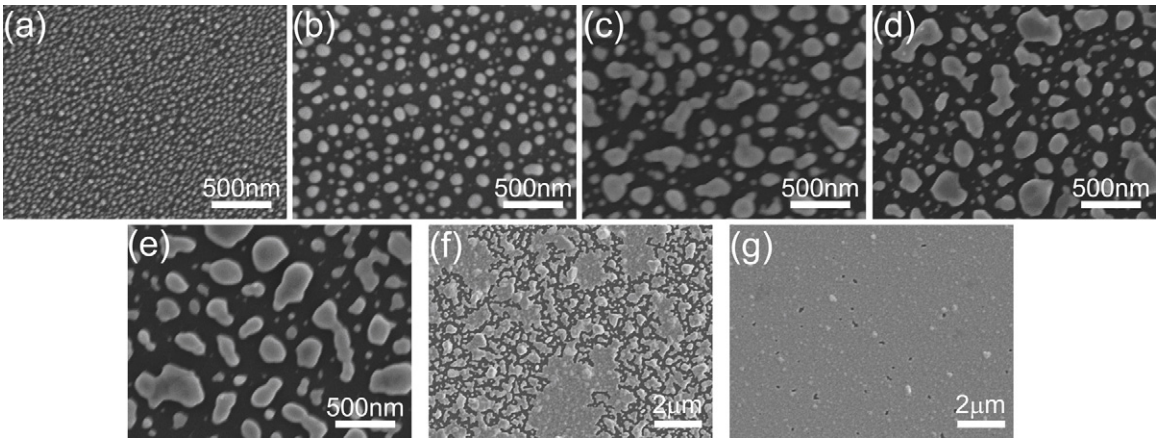

Fig. 1. SEM images of annealed Ag interlayers with different sputtering time, (a) 20 s, (b) 40 s, (c) 60 s, (d) 80 s, (e) 100 s, (f) 140 s and (g) 180 s.

technology, a-$Si_{1-x}C_x$:H prepared via PECVD is also a good candidate for the applications in Si-based electroluminescent or optoelectronic devices [31]. However, due to the recent blooming development of the modern LED and other advanced optoelectronic devices, more rigorous functional requests on the novel materials have been becoming the bottle-neck of the conventional a-$Si_{1-x}C_x$:H films processing research.

Therefore, we combined the SP light emission enhancement mechanism and the current a-$Si_{1-x}C_x$:H film deposition concept. In this study, the carbon-rich a-$Si_{1-x}C_x$:H films prepared by PECVD were coupled with both LSPs and PSPs generated by nano-structured Ag interlayers. The PL of the composite films was studied. In addition, the relationship between PL enhancement and SPs was also systematically investigated and uncovered.

2. Experimental procedures

Seven Ag films with different sputtering time (20 s, 40 s, 60 s, 80 s, 100 s, 140 s, and 180 s) were prepared on 2 cm × 1 cm silica substrates by DC magnetron sputtering in Ar ambience, labelled as S1-7, respectively. The thickness of Ag film deposited for 180 s is approximately 30 nm. Subsequent thermal annealing was carried out at 500 °C for 40 min in ambient N_2 to form Ag nanoparticles. The carbon-rich a-$Si_{1-x}C_x$:H films (thickness of ~120 nm), with a PL peak at ~480 nm, were deposited directly on the Ag interlayers. The deposition was carried out in an RF-PECVD system using SiH_4 (diluted to 10% in H_2) and C_2H_4 as the gas sources. The flow rates of H_2-diluted 10% SiH_4 and C_2H_4 were set at 20 and 10 sccm, respectively. More deposition details can be found in our previous report [32]. A reference sample of a pure a-$Si_{1-x}C_x$:H film was also prepared under the same condition to compare the PL of a-$Si_{1-x}C_x$:H films with Ag interlayer.

The thickness of a-$Si_{1-x}C_x$:H and Ag films, and the surface morphology of the annealed Ag interlayers were obtained by field-emission scanning electron microscopy (S4800, Hitachi). The full PL spectra were obtained with a fluorescence spectrometer (FLS920, Edinburgh Instruments Ltd.) using a 325 nm UV xenon lamp as the excitation source. To avoid reflecting the excitation light into the detector, the samples were maintained at 60° to the incident plane during the PL spectra measurement. The extinction spectra of all samples were measured using a UV–vis spectrometer (TU-1901, Beijing Purkinje General Instrument CO., Ltd.). The Image-Pro Plus 5.0 software was used to analyze the SEM images, in order to obtain the average Ag nanoparticle area and the surface area coverage of Ag interlayers.

3. Results and discussion

The microstructural characteristics of the annealed Ag interlayers were found to vary dramatically with the sputtering time, as shown in Fig. 1. Due to the irregular shape of Ag nanoparticles, we estimated the average diameter assuming all nanoparticles were of spherical shape. The average Ag nanoparticle area and diameter, and the surface area coverage of Ag interlayers are listed in Table 1. With the increase of the sputtering time, the size of Ag nanoparticles and the surface area coverage increased significantly. The Ag interlayers deposited for 140 s and 180 s became more continuous,

Table 1
The average Ag nanoparticle area and diameter, and the surface area coverage of Ag interlayers.

Ag sputtering time (s)	Average nanoparticle area (nm^2)	Average diameter (nm)	Surface area coverage
20	319	20.14	34.95%
40	1270	40.21	34.45%
60	2242	53.43	37.12%
80	2700	58.63	41.71%
100	4518	75.85	43.73%
140	–	–	69.00%
180	–	–	99.55%

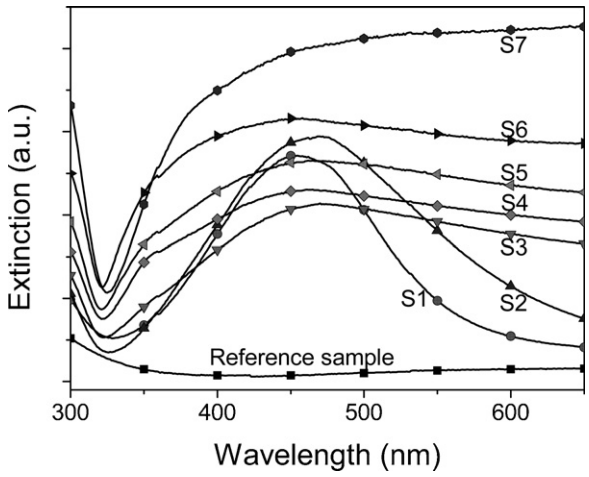

Fig. 2. The extinction spectra of S1-7 and the reference sample.

with surface area coverage of ~ 69% and 100%, respectively. There are two components of the electromagnetic field associated with plasmon resonances in Ag nanoparticles: a non-radiative absorbing component and a near-field component that evolves into radiative far-field scattering [33]. The sum of the true absorption and the scattering represents the total extinction of light. The size and the shape of the particles as well as the dielectric function of the surrounding medium determine the frequency and the strength of the plasmon resonance. In our case, the dielectric medium of the Ag interlayers, namely a-$Si_{1-x}C_x$:H films and silica slides, remained the same. The Ag nanoparticles of S1 are spherical shape with an average size of 20 nm. As shown in Fig. 2, the extinction spectrum of S1 is symmetrical and its full width at half maximum is smaller than those of S2-7. With the sputtering time increased to 40 s, the Ag nanoparticles began to merge together, presenting

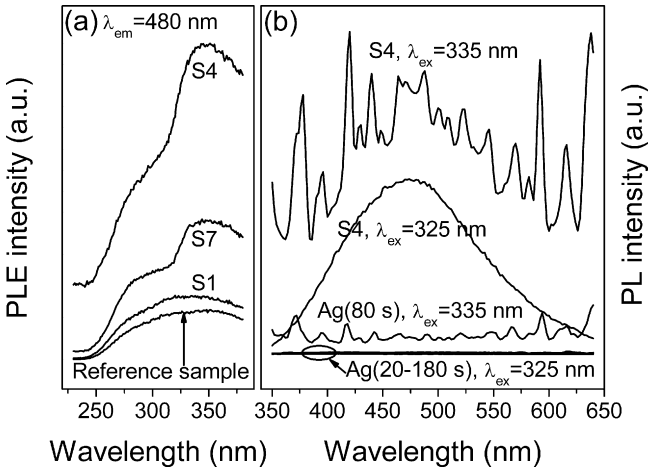

Fig. 3. (a) PL excitation spectra of S1, S4, S7 and the reference sample monitoring 480 nm emission. (b) The PL spectra of S4 and its Ag interlayer under 325 and 335 nm excitation. And the PL spectra of Ag interlayers deposited for different sputtering time under 325 nm excitation.

ellipsoidal and dumbbell-shape characteristic. For samples S3-6, more Ag nanoparticles connected and overlapped with each other to form larger nanoparticles with more irregular shape and wider size distribution. When the sputtering time was increased to 180 s (sample S7), the Ag nanoparticles almost formed a continuous film with large Ag particles and rough surface. Due to the large varieties of the size and the shape of the Ag nanoparticles, different SP modes of different resonance energies led to broad extinction spectra for S3-7 [13]. In comparison, the a-$Si_{1-x}C_x$:H reference sample presented a low absorption over the whole spectra.

Fig. 3(a) shows the PL excitation spectra of S1, S4, S7 and the reference sample monitoring the a-$Si_{1-x}C_x$:H emission maximum at 480 nm. A broad excitation band between 280 and 380 nm was observed for the reference sample. Within this region, the PL spectra remained almost unchanged when the reference sample was excited with light of different wavelengths. For the SP-enhanced samples, the excitation band further rose between 330 and 380 nm due to SPs generated in the Ag interlayers. However, it is not suitable to excite the SP-enhanced samples by excitation light within this band. For example, when S4 was excited at 335 nm, the PL spectra (Fig. 3(b)) exhibited disordered sharp peaks over the a-$Si_{1-x}C_x$:H emission band. The result indicated that SPs was excited by the 335 nm incident light instead of a-$Si_{1-x}C_x$:H PL, and the SPs induced 'side effect' on the a-$Si_{1-x}C_x$:H PL. The disordered PL spectra (shown in Fig. 3(b)) from the naked Ag interlayer without a-$Si_{1-x}C_x$:H film confirmed such 'side effect'. As shown in Fig. 2, the extinction spectra of all SP-enhanced samples show dips at around 325 nm. It means that the Ag interlayers are almost transparent to the 325 nm light, thus SPs can be hardly excited at this wavelength. As shown in Fig. 3(b), no PL was detected from all the annealed Ag films when excited by 325 nm incident light. And the PL spectra from S4 showed smoother characteristic than that excited by 335 light. This phenomenon implies that the scattering or the reflection of the excitation light by Ag films can be excluded by using 325 nm light. Therefore, all the following PL results were obtained by using 325 nm incident light.

The PL spectra of all the samples are shown in Fig. 4(a). The integrated PL enhancement factor is defined as the ratio of the integrated PL intensity of the SP-enhanced sample to that of the reference sample. The enhancement factor as a function of the sputtering time is illustrated in Fig. 4(b). It is well known that the PL quenching effect occurs at rather short distance (<10 nm) near the light-emitting material/metal interface [18,34]. However, in this study, the PL of all samples was eventually enhanced on the a-$Si_{1-x}C_x$:H films of ~120 nm in thickness, as shown in Fig. 4(a and b). Therefore, the PL quenching at the interface can be neglected. The enhancement factor was found to be sensitive to the Ag sputtering time. It firstly increased with the sputtering time, subsequently reached a maximum value of 3.3 for S5 (sputtering time 100 s), and then decreased slowly. The average Ag nanoparticle size and the surface area coverage of Ag interlayers for S5 were 76 nm and ~44%, respectively. The inset of Fig. 4(b) shows the PL image of S5 taken by a conventional digital camera under the room light. All eight samples exhibited a blue–green RT PL visible to the naked eye. In our previous report, we have confirmed the multiphase structure and PL mechanism of the carbon-rich a-$Si_{1-x}C_x$:H films used in this work, which consist of hydrogenated sp^3 Si–C network and amorphous carbon clusters [32]. The origin of PL is the radiative recombination of electron–hole pairs within sp^2 bonded carbon clusters in a sp^3 bonded Si–C matrix. Overall, the PL enhancement via SPs is the result of two sequential processes [2]. Firstly, when the excited dipole energies of the light-emitting layer and the SP energy of the metal are similar, the excited dipole energies can be transferred into SP modes of the metal. As indicated in Figs. 2 and 4, the emission band of a-$Si_{1-x}C_x$:H at about 480 nm overlaps the SP resonance band of the Ag interlayers. So the excited dipole energies of the a-$Si_{1-x}C_x$:H films and the SP energy of the Ag interlayer are similar, then the energies can be transferred into SP modes. Secondly, the SPs localized in metal nanoparticles can radiate into light directly and efficiently [13]. The scattering component of the nanoparticle extinction is a measure of the extent to which the plasmons can radiate into the far-field [35]. Larger Ag nanoparticles result in larger scattering cross section and higher scattering efficiency [33]. As shown in Fig. 1 and Table 1, the longer sputtering time led to the Ag nanoparticles with larger dimension. Therefore, the PL enhancement factor rose with the increasing sputtering time,

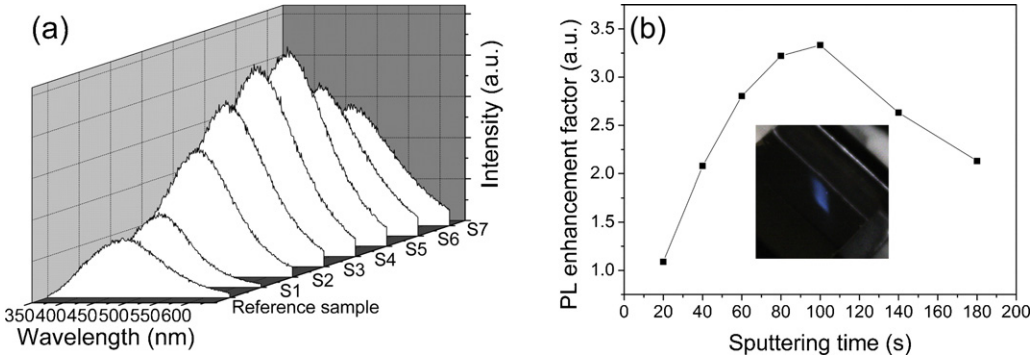

Fig. 4. (a) PL spectra of S1-7 and the reference sample. (b) The integrated PL enhancement factors of S1-7 as a function of the sputtering time. The inset shows the PL image of S5 taken by a conventional digital camera under the room light.

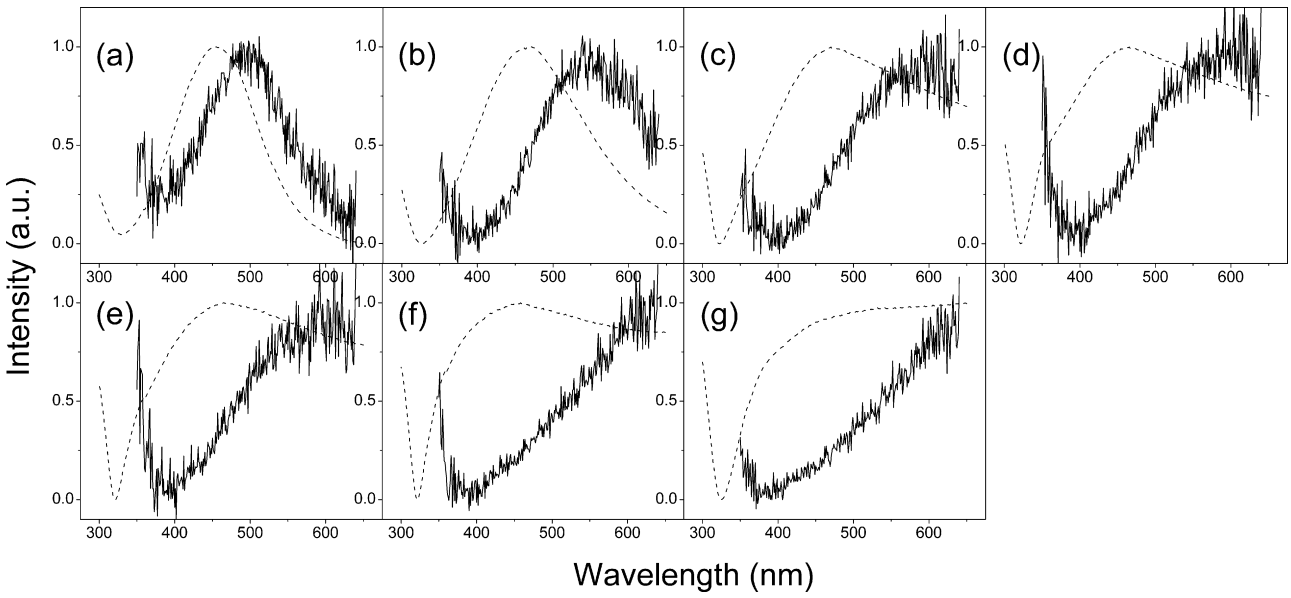

Fig. 5. The normalized wavelength-dependent PL enhancement factors (solid lines) and extinction spectra (dash lines) of (a) S1, (b) S2, (c) S3, (d) S4, (e) S5, (f) S6 and (g) S7.

and reached the maximum for S5. For the SPs propagating on a planar interface, the nanostructure or the roughness of the metal layer allows SPs of high momentum to scatter, lose their momentum, and couple to radiated light. When the Ag nanoparticles fused and formed a continuous Ag interlayer (S6 and S7), the reduction of surface roughness attenuated the scattering of SPs, and part of the SP energy would be thermally dissipated [2]. Therefore the enhancement factors of S6 and S7 became lower than that of S5. The variation of integrated PL enhancement factor with Ag sputtering time indicated that the enhancement was dominated by the scattering of LSPs and PSPs by Ag interlayers in our case.

The wavelength-dependent PL enhancement factor (abbreviated as WPLEF) is defined as the ratio of the PL intensity of the SP-enhanced sample to that of the reference sample at each wavelength, shown in Fig. 5 (solid lines). We noted that the WPLEF curves were similar to the corresponding extinction spectra, especially for the LSP enhanced samples (S1–S5). The phenomenon was also observed from the a-C:H films in our previous study, when the film thickness was larger than 90 nm [11]. The WPLEF and the extinction spectra (dash lines) were normalized and plotted together in Fig. 5 for further analysis. The curves of these two spectra resembled each other in shape but with shifts of dozens of nanometer. Such red shift depends on the Ag nanoparticle size. The increased Ag sputtering time led to bigger nanoparticle size and a more remarkable shift. The observed spectral shift between the WPLEF curves and the extinction spectra is believed to be correspondent to the difference between the near- and far-field measured plasmon resonance peak positions. The measure of the plasmonic response of a metallic nanoparticle or nanostructure commonly used involves its far-field quantities, such as absorption, scattering, and extinction, and its near-field properties, such as the intensity and spatial distribution of its electromagnetic field enhancements [36]. The electromagnetic field enhancement leads to an increased excitation rate and radiative recombination rate of the electron–hole pairs in the light-emitting layer [37]. Since the PL enhancement involves the near-field exciton-plasmon interaction, the WPLEF curves represent the near-field properties of the SPs. The localized plasmons of metallic nanoparticles and nanostructures display a universal phenomenon, which is that upon optical excitation, the maximum near-field enhancements occur at lower energies than the maximum of the corresponding far-field spectrum [36]. Such red shift of the near-field peak energies with respect to the far-field peak energies is known to depend upon the size of the particles, with larger particles displaying a more marked shift [38,39]. The above phenomenon was consistent with the red shift of WPLEF curves. Therefore, the shape resemblance and the peak shift between the WPLEF curves and the extinction spectra suggested that the obtained PL enhancement was attributed to the coupling between electron-hole pairs in a-$Si_{1-x}C_x$:H films and the LSPs and PSPs generated at the Ag/a-$Si_{1-x}C_x$:H interface.

4. Conclusions

The blue–green light emission of carbon-rich a-$Si_{1-x}C_x$:H films was successfully enhanced by coupling through LSPs and PSPs supported by nano-structured Ag interlayers. The enhancement factor was found to firstly increase with the Ag nanoparticle size, subsequently reach a maximum value of 3.3 when the average Ag nanoparticle size and the surface area coverage of Ag interlayers were 76 nm and 44%, respectively, and finally decrease as the Ag interlayers became continuous. The results indicated that the enhancement was dominated by the scattering of LSPs and PSPs by Ag interlayers. The relationship between the PL enhancement factors curves and the corresponding extinction spectra was attributed to the near-field enhancement and far-field extinction, respectively. Since the carbon-based films, such as amorphous carbon films and diamond-like carbon films, have similar microstructure and PL mechanism to those of the carbon-rich a-$Si_{1-x}C_x$:H films, coupling with SPs has therefore been proven to be a promising way to enhance the light emission efficiency of carbon-based films which can also be utilized for the large-area solid-state lighting applications.

Acknowledgements

This work was financially supported by the National Basic Research Program of China - 973 Program (grant 2007CB613403), the Foundation of the scientific research base development program (grant KYJD09014), the National natural science foundation of China (grant 51103128) and the Independent research program of Zhejiang University (grant 2011QNA4004).

References

[1] K. Okamoto, Y. Kawakami, IEEE J Sel. Top. Quantum Electron. 15 (2009) 1199–1209.
[2] W.L. Barnes, Nat. Mater. 3 (2004) 588–589.
[3] B.H. Kim, C.H. Cho, J.S. Mun, M.K. Kwon, T.Y. Park, J.S. Kim, C.C. Byeon, J. Lee, S.J. Park, Adv. Mater. 20 (2008) 3100–3104.
[4] C.Y. Cho, M.K. Kwon, S.J. Lee, S.H. Han, J.W. Kang, S.E. Kang, D.Y. Lee, S.J. Park, Nanotechnology 21 (2010) 205201.
[5] Y. Kuo, S.Y. Ting, C.H. Liao, J.J. Huang, C.Y. Chen, C. Hsieh, Y.C. Lu, K.C. Shen, C.F. Lu, D.M. Yeh, J.Y. Wang, W.H. Chuang, Y.W. Kiang, C.C. Yang, Opt. Express 19 (2011) 914–929.
[6] Z.L. Schaefer, D.D. Vaughn, R.E. Schaak, J. Alloys Compd. 490 (2011) 98–102.
[7] K. Aslan, M.J.R. Previte, Y.X. Zhang, C.D. Geddes, Anal. Chem. 80 (2008) 7304–7312.
[8] J. Lin, A. Mohammadizia, A. Neogi, H. Morkoc, M. Ohtsu, Appl. Phys. Lett. 97 (2010) 221104.
[9] P.M. Kadam, N.L. Tarwal, P.S. Shinde, S.S. Mali, R.S. Patil, A.K. Bhosale, H.P. Deshmukh, P.S. Patil, J. Alloys Compd. 509 (2011) 1729–1733.
[10] D.J. Qiu, Z.F. Wan, X.K. Cai, Z.J. Yuan, L.A. Hu, B.P. Zhang, C.F. Cai, H.Z. Wu, Opt. Express 18 (2010) 23385–23394.
[11] Z. Li, X. Li, Z.H. Ren, Q. Gao, X.W. Zhang, G.R. Han, Opt. Express 19 (2011) 17935–17943.
[12] K. Okamoto, I. Niki, A. Shvartser, Y. Narukawa, T. Mukai, A. Scherer, Nat. Mater. 3 (2004) 601–605.
[13] D.M. Yeh, C.F. Huang, C.Y. Chen, Y.C. Lu, C.C. Yang, Nanotechnology 19 (2008) 345201.
[14] P.H. Cheng, D.S. Li, J.X. Wang, D.R. Yang, Appl. Surf. Sci. 257 (2011) 5591–5594.
[15] D.Y. Lei, H.C. Ong, Appl. Phys. Lett. 91 (2007) 021112.
[16] P.H. Cheng, D.S. Li, Z.Z. Yuan, P.L. Chen, D.R. Yang, Appl. Phys. Lett. 92 (2008) 041119.
[17] J. Li, H.C. Ong, Appl. Phys. Lett. 92 (2008) 121107.
[18] P.H. Cheng, D.S. Li, X.Q. Li, T. Liu, D.R. Yang, J. Appl. Phys. 106 (2009) 063120.
[19] B.J. Lawrie, R.F. Haglund Jr., R. Mu, Opt. Express 17 (2009) 2565–2572.
[20] A.M. Hanel, M. Kunle, P. Loper, S. Janz, A.W. Bett, Sol. Energy Mater. Sol. Cells 94 (2010) 1942–1946.
[21] Q.J. Cheng, S. Xu, J.D. Long, Z.H. Ni, A.E. Rider, K. Ostrikov, J. Phys. D: Appl. Phys. 41 (2008) 055406.
[22] J. Xu, L. Yang, Y.J. Rui, J.X. Mei, X. Zhang, W. Li, Z.Y. Ma, L. Xu, X.F. Huang, K.J. Chen, Solid State Commun. 133 (2005) 565–568.
[23] C. Song, Y.J. Rui, Q.B. Wang, J. Xu, W. Li, K.J. Chen, Y.H. Zuo, Q.M. Wang, J. Alloys Compd. 509 (2011) 3963–3966.
[24] L. Wang, J. Xu, T.F. Ma, W. Li, X.F. Huang, K.J. Chen, J. Alloys Compd. 290 (1999) 273–278.
[25] B.P. Swain, B.S. Swain, S.H. Park, N.M. Hwang, J. Alloys Compd. 480 (2009) 878–881.
[26] B.P. Swain, R.O. Dusane, Mater. Lett. 61 (2007) 4731–4734.
[27] K. Fujie, A. Ito, R. Tu, T. Goto, J. Alloys Compd. 502 (2010) 238–242.
[28] E.N. Kalabukhova, S.N. Lukin, D.V. Savchenko, B.D. Shanina, A.V. Vasin, V.S. Lysenko, A.N. Nazarov, A.V. Rusavsky, J. Hoentsch, Y. Koshka, Phys. Rev. B 81 (2010) 155319.
[29] Z.D. Sha, X.M. Wu, L.J. Zhuge, Vacuum 79 (2005) 250–254.
[30] Y.H. Wang, J. Lin, C.H.A. Huan, Mater. Sci. Eng. B: Solid State Mater. Adv. Technol. 95 (2002) 43–50.
[31] T.F. Ma, J. Xu, J.F. Du, W. Li, X.F. Huang, K.J. Chen, J. Appl. Phys. 88 (2000) 6408–6412.
[32] Z. Li, J. Zhang, H.Y. He, J.C. Bian, X.W. Zhang, G.R. Han, Phys. Status Solidi (a): Appl. Mater. 207 (2010) 2543–2548.
[33] D.D. Evanoff, G. Chumanov, J. Phys. Chem. B 108 (2004) 13957–13962.
[34] C.S. Yun, A. Javier, T. Jennings, M. Fisher, S. Hira, S. Peterson, B. Hopkins, N.O. Reich, G.F. Strouse, J. Am. Chem. Soc. 127 (2005) 3115–3119.
[35] J.R. Lakowicz, Anal. Biochem. 337 (2005) 171–194.
[36] J. Zuloaga, P. Nordlander, Nano Lett. 11 (2011) 1280–1283.
[37] X.D. Zhou, X.H. Xiao, J.X. Xu, G.X. Cai, F. Ren, C.Z. Jiang, EPL 93 (2011) 57009.
[38] G.W. Bryant, F.J.G. De Abajo, J. Aizpurua, Nano Lett. 8 (2008) 631–636.
[39] B.M. Ross, L.P. Lee, Opt. Lett. 34 (2009) 896–898.